Composites Part A 109 (2018) 31–47

Contents lists available at ScienceDirect

Composites Part A

journal homepage: www.elsevier.com/locate/compositesa

Uniaxial strength of a composite array of overlaid and aligned prepreg platelets

Sergii G. Kravchenko*, Drew E. Sommer, R. Byron Pipes

Purdue University, Composites Manufacturing and Simulation Center, Indiana Manufacturing Institute, 1105 Challenger Avenue, Suite 100, West Lafayette, IN 47906, United States

ARTICLE INFO

Keywords:
A. Discontinuous reinforcement
B. Strength
C. Damage mechanics
C. Cohesive interface modeling
Platelet

ABSTRACT

The tensile strength of a discontinuous composite system consisting of aligned, unidirectional prepreg platelets is predicted by performing progressive damage analyses in a periodic representative volume element. Interlaminar and in-plane damage mechanisms are combined to yield failure characteristics of the meso-structure. The length-to-thickness ratio of the platelet was found to be the primary variable for control of system strength and failure mode. A critical platelet aspect ratio was determined as that ratio wherein system strength is maximized. Further, composite strength variability was shown to be vary inversely with aspect ratio, while attaining a minimum at the critical aspect ratio.

1. Introduction

Formability and structural characteristics of a fiber-reinforced composite define the possible application for the material. Conventional advanced composite materials consist of multi-axial laminates constructed of lamina of collimated, continuous fibers (CF) pre-impregnated with polymeric matrices. The composite lamina preform is termed “prepreg”. However, complex three-dimensional geometries often cannot be efficiently fabricated as continuous fiber laminates. Yet well dispersed, short fiber molding of these geometries does not yield the superior structural performance of CF systems since fiber length and volume fraction are significantly lower than that of the CF systems. Recently, a modified material form has been introduced that provides for controlled fiber length and fiber volume fractions in the range of 0.5–0.6. These materials are fabricated by transforming CF prepreg tape, through a slitting and cutting procedure, into platelets with a prescribed length, L_p, and width, w_p, while the platelet thickness, t_p, is the prepreg tape thickness. These platelets are then compression or transfer molded into complex geometries appropriate for structural elements. Application of a prepreg platelet-molded composite requires basic knowledge of its performance. Effective/macroscopic properties of a heterogeneous composite system emerge from the complex collective response of the interacting phases, which depends on the material structure and the local properties of each constituent phase. The material structure is a collective arrangement of the phases at the next scale above that of an individual phase. The structure is characterized [1] by the geometrical arrangement of constituents in space (known as material morphology), proportions (fractions) and shapes of the constituent phases. A systematic knowledge of the material structure-property relationship [2] is needed to understand the origins of apparent properties from the material structure and to achieve the desired combination of properties.

Meso-scale morphology is dominant for the properties of a prepreg platelet-molded composite system, meaning the scale where individual platelets are distinguishable. A composite system of platelets fabricated from unidirectional (UD) CF prepreg is a hierarchical system with two levels of recognized scale. As pointed out by Lakes [3], a structure may be present on many scales, but the largest structural element scale controls the effective response of the material system. When continuous fibers are arranged in a collimated, high fiber volume fraction geometry such as in a CF prepreg and that system is cut into platelets that contain fibers of identical length, individual fibers may not be expected to control system strength. Rather, the properties of a platelet based composite are determined by the platelet-scale heterogeneities. Therefore, it is the morphology dependent three dimensional platelet-to-platelet stress transfer governs the failure mechanisms and, consequently, the effective composite strength.

The geometric meso-scale of the platelet composite can be irregular and disordered, having platelets arranged in “random” and varying patterns at various orientations with respect to one another in a semi-laminated manner, as schematically shown in Fig. 1. Irregular disordered meso-structures resulting from uncontrolled platelet deposition and further molding are complex and both property measurements and predictions have shown their large variations [4–13]. The primary

* Corresponding author.
E-mail address: skravche@purdue.edu (S.G. Kravchenko).

https://doi.org/10.1016/j.compositesa.2018.02.032
Received 22 October 2017; Received in revised form 18 February 2018; Accepted 22 February 2018
Available online 24 February 2018
1359-835X/

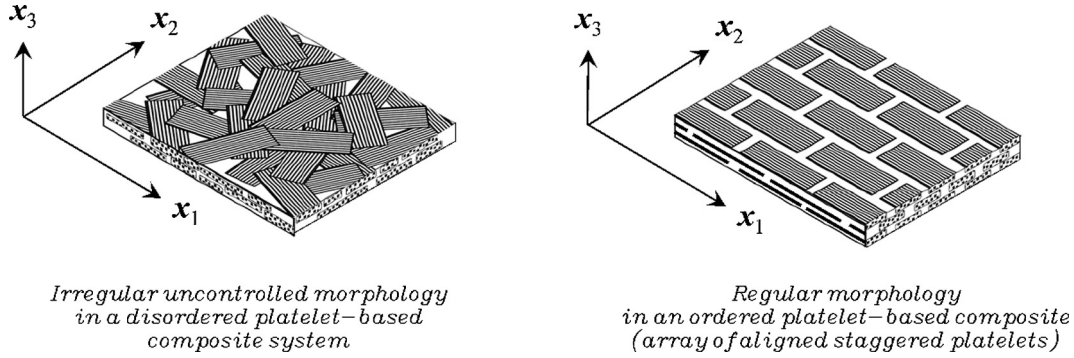

Fig. 1. Schematics of an irregular and regular morphologies of a platelet-based composite system.

observations from the previous studies were that (a) the strength of a platelet-molded material system increased with platelet length (L_p) for a constant thickness (t_p) [4,5,7], (b) the failure was observed to be either platelet pullout or platelet split or rupture, and (c) thinner tape allowed for the improved effective properties [11,12]. Large variability in the experimental data was suggested [14] to be caused by the non-deterministic distribution of arrangement and overlap lengths of platelets.

A composite system with regular morphology must have some repeatable pattern for elements accommodation in space. For instance, all platelets can be aligned and staggered in a certain manner to create a regular morphology, as shown in Fig. 1. Regular morphologies can be engineered, meaning achieved with a specific manufacturing procedure. Simpler geometrical arrangement of platelets defines a "simpler morphology", which actually corresponds to a more ordered composite system, or a structure of a superior hierarchical organization. Ordered system morphology grants superior effective performance characteristics. Besides, if regular morphologies can be manufactured, they represent independent composite systems, which require their own computational predictive models.

In the present work, the authors examine a simple geometry of a meso-structure with many platelets in order to identify stress transfer and strengths as a function of meso-structure geometry (morphology) and platelet aspect ratio in the absence of orientation disorder. An idealized strictly periodic system of aligned staggered prepreg platelets is herein considered. A simple morphology may not be directly useful for quantitative predictions of the effective properties of more complex morphologies but it can provide an insight, qualitative understanding and easier interpretation of common phenomena responsible for the effective performance of various types of morphologies. This work thereby provides the necessary foundation to study the structure-property relationship in more complex irregular and stochastic meso-structures wherein platelet fiber orientation and overlap geometries are more typical of systems resulting from uncontrolled deposition and molding.

Natural [15] and engineered discontinuous composite systems of layered and staggered platelets made of different materials were previously studied for elastic response [16–20] and ultimate strength prediction, based on simplified stress analysis [21–24] or progressive failure analysis (PFA) [25–30]. In these systems, platelets (also termed bricks, strands, flakes, or chips by different authors) were separated by adhesive layers (matrix, mortar, resin). Predictive models for such material systems relate the composite morphology, constituent properties, and platelet geometry to the macroscopic mechanical response of a composite for the purpose of decision making on material selection and processing limits. Both models from [26,27] gave insight to the deformation and failure of platelet arrayed composites, though with limitations on predictive capabilities from inherent assumptions. Models from Refs. [26,27] were plane stress and shear-lag based, implying there were no interlaminar peel stresses allowed at the platelet-to-platelet interfaces, the mismatch in Poisson's ratio between platelet and adhesive layer was not accounted for, besides the platelets were considered isotropic. The authors of [25,28–30] assumed that platelets could not experience breakage and excluded such failure mode from their model.

The focus of this paper is to develop a comprehensive computational model to quantify the structure-property relationship in a composite system of overlaid and aligned prepreg platelets under uniform uniaxial tensile loading in the displacement control. The sub-scale modeling was used for the analysis of three-dimensional local stress transfer and damaged deformation to failure in the composite system. The direct computational homogenization [31,32] was used to yield the effective composite stress at any loading increment. A strictly periodic meso-scale geometry was considered so that a unit cell could exist to adequately represent the heterogeneity of the system. A unit cell was chosen as a representative volume element (RVE) [33] thus making the periodic boundary conditions appropriate to the RVE. The direct finite element method was used to analyze the RVE in ABAQUS/Standard (Implicit). A continuum damage mechanics model for the orthotropic platelet damage modes was coupled with a cohesive zone model at the inter-platelet planes to capture the disbonding between platelets and thereby address the two competing failure mechanisms in the system. The study of the structure-property relationships in the platelet-arrayed composite system revealed that a *"critical platelet length-to-thickness ratio" for the chosen composite morphology* exists to maximize the effective composite strength. This dimensionless parameter is shown to control the failure modes and, consequently, attainable macroscopic composite strength. Variability in morphology of a platelet-based composite is shown to control the strength variability for smaller length-to-thickness platelet aspect ratio. The results also suggest that strength variability caused by meso-morphology in a platelet-based composite system can be mitigated by increasing the platelet length-to-thickness ratio.

2. RVE-based computational model for the progressive failure analysis in a platelet-arrayed composite

2.1. Assumptions for the failure analysis of an array of aligned platelets

Three primary assumptions are employed in this work for the progressive failure analysis in a platelet-arrayed composite system: (i) geometrical idealization of platelet arrangement, i.e. composite heterogeneous meso-scale morphology; (ii) idealization of stress-carrying capacity of the composite elements; (iii) idealization of elementary damage events in the composite system.

The composite system is a collection of UD CF prepreg platelets that have been systematically arranged. It is assumed that platelets are laid side by side and parallel to one another in strictly periodic, but staggered planar arrays with their length direction (coincident with the fiber, or the "*1*"-preferential direction) along the global x_1-direction. Thin matrix layers are assumed to separate the platelets in the thickness direction, x_3. The (x_1x_2)-planar arrays are organized to replicate in every other layer through the stack thickness direction (x_3). Perfect

bonding between platelets and matrix layers is assumed. All platelets are assumed to possess the same dimensions (length, width, thickness) in a given RVE and matrix layer has the same thickness.

The three-dimensional stress transfer in the composite system must be modeled to capture the possible failure modes. The platelets are assumed to carry the in-plane stress components (σ_{11},σ_{22},σ_{12}), since the platelet thickness, t_p, is taken to be much smaller than its planar dimensions (w_p, L_p). The stress transfer between platelets is assumed to be entirely through the adhesive layers in overlap regions. The matrix layer is assumed to transmit out-of-plane transverse shear (σ_{13},σ_{23}) and normal peel stress (σ_{33}) between the platelets, but not to sustain in-plane (membrane) stretching and shear stress. The assumption of the matrix layer supporting no in-plane stress is acceptable when the polymer is (i) much more compliant and (ii) relatively thin compared to the adherent (platelet) and is consistent with typical shear lag analyses. No attempt was made to distinguish between the adhesive and cohesive types of failure in the matrix layer due to its small thickness. In this way, the matrix layer was considered not as an independent constituent with its own set of mechanical properties along with adhesive/platelet interface, but rather as a platelet-to-platelet interface. This approach seems reasonable for high platelet volume fractions (above 0.8), but could become an over-simplification if the matrix layer thickness were relatively large and the platelet volume fraction small. For simplicity, no load was assumed to be transferred through the platelet ends, i.e. there was no in-plane normal stress transferred through the edges of the platelets (platelet ends were considered dis-bonded from the matrix). This assumption corresponds to the Cox's shear-lag model [34] for a short fiber composite.

Ultimate failure of a heterogeneous composite system is preceded by the successive evolution and interaction of local damage in platelets and matrix layer, and occurs after enough sub-critical damage is gradually accumulated for the system to lose its load carrying capacity. The following fractures are considered as sub-scale damage in an array of prepreg platelets: (a) a platelet longitudinal split along the fibers (transverse, or intra-platelet damage); (b) platelet-to-platelet interfacial disbonding/delamination (inter-platelet damage, or platelet pull-out), and (c) fiber breakage in a platelet (trans-platelet damage, or platelet rupture). The damage in a platelet is idealized as damage in a UD CF ply at the meso-scale [35,36]. The modeling of dis-bonding between the platelets is similar to previous modeling of the interlaminar damage (delamination) between the individual plies of a laminate [37–39].

2.2. Finite-element implementation of an RVE-based computational model

RVE-based analysis is herein used to predict the effective failure characteristics of the platelet-arrayed composite system. Each RVE represents a specific choice in meso-structure geometry of the composite (platelet arrangement) and thereby provides a tool to examine the different physical mechanisms leading to failure as the composite morphology is varied. The RVE contains four platelets located in three layers, as sketched in Fig. 2. Two platelets make up the central layer, while the half-thicknesses of the other two platelets are in the two outer layers. In order to achieve periodic geometries, platelets extending past the right boundary of the RVE appear in the left boundary of the RVE, in similar fashion for other boundaries. Geometrical parameters of a given platelet (length, L_p, width, w_p, and thickness, t_p) are shown in Fig. 2. The RVE dimensions thus are: $L_x = L_p + \delta_x$, $L_y = 2w_p + 2\delta_y$, $L_z = 2(t_p + t_{coh})$ with δ_x,δ_y, and t_{coh} being the spacing between the platelets (matrix layer thickness), shown in Fig. 2. The analysis is carried out with a commercial implicit finite element code ABAQUS/Standard 6.14-1.

The geometrical dimensions of a platelet ($t_p \ll L_p$, w_p) suggest to use the shell formulation to achieve computational efficiency. Besides, the shell formulation allows for a coarser finite element discretization as compared to the three-dimensional stress formulation. The platelets are modeled with homogeneous continuum shells (SC8R) with the stiffness matrix of a plane stress orthotropic material undergoing damage, utilizing the ABAQUS built-in anisotropic continuum damage mechanics based constitutive model. Isotopic matrix layers of small thickness ($t_{coh} = 5\,\mu m$) in the overlaps of platelets are modeled with cohesive elements (COH3D8) obeying the traction-separation law. Schematics of stress carrying capacity of both composite constituent phases are shown in Fig. 2. Node sharing between the platelets and adhesive layers is insured by modeling the RVE as a single part solid (in ABAQUS jargon) to avoid using tie constraints. Periodic boundary conditions (PBC) in the displacement difference form are applied to the RVE faces as formulated by Suquet [32], which allows for the non-linear analysis with local material softening.

2.3. Constitutive models for progressive damage/failure analysis of a platelet ensemble

Damage was assumed as a collection of irreversible distributed changes in the material from loading which affect its mechanical response [40]. Stiffness reduction models were used so that the effects of sub-scale damage at the composite element level were lumped into the macroscopic internal damage variables [41,42]. The damage variables modified the material properties based on a strain-softening formulation of the stress-strain relationship and were defined for each elementary degradation mechanism. The pattern of the damage variables effectively represented a macroscopic crack, meaning a region with no stiffness in a specific damage mode and thereby, no stress carrying capacity for that mode in a fully degraded state. The platelet damage modes and the damageable interfaces between the platelets were treated with different computational damage theories. The elastic-brittle continuum damage mechanics (CDM) model with orthotropic damage for platelets was coupled with the discrete damage theory with isotropic damage (cohesive zone modeling) to capture the dis-bonding between platelets. Direct coupling of the two models was accomplished by incorporating both damage models within a single finite element model. The orthotropic platelets were assumed to be made of AS4/PEEK CF UD tape with elastic and failure properties [43] given in Table 1, and fracture properties [44] given in Table 2.

2.3.1. Damaged response of a platelet

The platelet is treated as an orthotropic homogenized continuum in which in-plane damage is the result of the biaxial state of stress. Orthotropic damage was modeled by the evolution of several internal variables, d_{ij}, which control the systematic reduction of the orthotropic compliance matrix of the material. The phenomenological [45], local [46] CDM-based model implemented in ABAQUS/Standard [36,47] was used to simulate the degraded response of each platelet, as given by Eq. (1):

$$\begin{Bmatrix} \epsilon_{11} \\ \epsilon_{22} \\ 2\,\epsilon_{12} \end{Bmatrix} = \boldsymbol{H}(\boldsymbol{d}) \begin{Bmatrix} \sigma_{11} \\ \sigma_{22} \\ \sigma_{12} \end{Bmatrix}, \tag{1}$$

where $\boldsymbol{H}(\boldsymbol{d})$ is the damaged compliance matrix of platelet material and $\boldsymbol{d}$ is the vector of damage variables, both are given in Eq. (2). Herein, d_{11} reflects the damage in the fiber direction, d_{22} accounts for the damage in the second preferential direction, and d_{12} is the parameter for in-plane shear damage that depends on the damage variables d_{11} and d_{22} [36]. The damage variables are monotonically increasing functions in the range of $0 \leqslant d_{ij} \leqslant 1$, with $d_{ij} = 0(i,j = 1-2)$ corresponding to the initial undamaged material and $d_{ij} = 1(i,j = 1-2)$ representing a state of complete loss of integrity with no stress can be transferred.

$$\boldsymbol{H}(\boldsymbol{d}) = \begin{bmatrix} \frac{1}{(1-d_{11})E_{11}} & -\frac{\nu_{21}}{E_{22}} & 0 \\ -\frac{\nu_{12}}{E_{11}} & \frac{1}{(1-d_{22})E_{22}} & 0 \\ 0 & 0 & \frac{1}{(1-d_{12})G_{12}} \end{bmatrix}, \boldsymbol{d} = \begin{Bmatrix} d_{11} \\ d_{22} \\ d_{12} \end{Bmatrix} \tag{2}$$

The formulation of the damaged compliance matrix, $\boldsymbol{H}(\boldsymbol{d})$, utilized in this

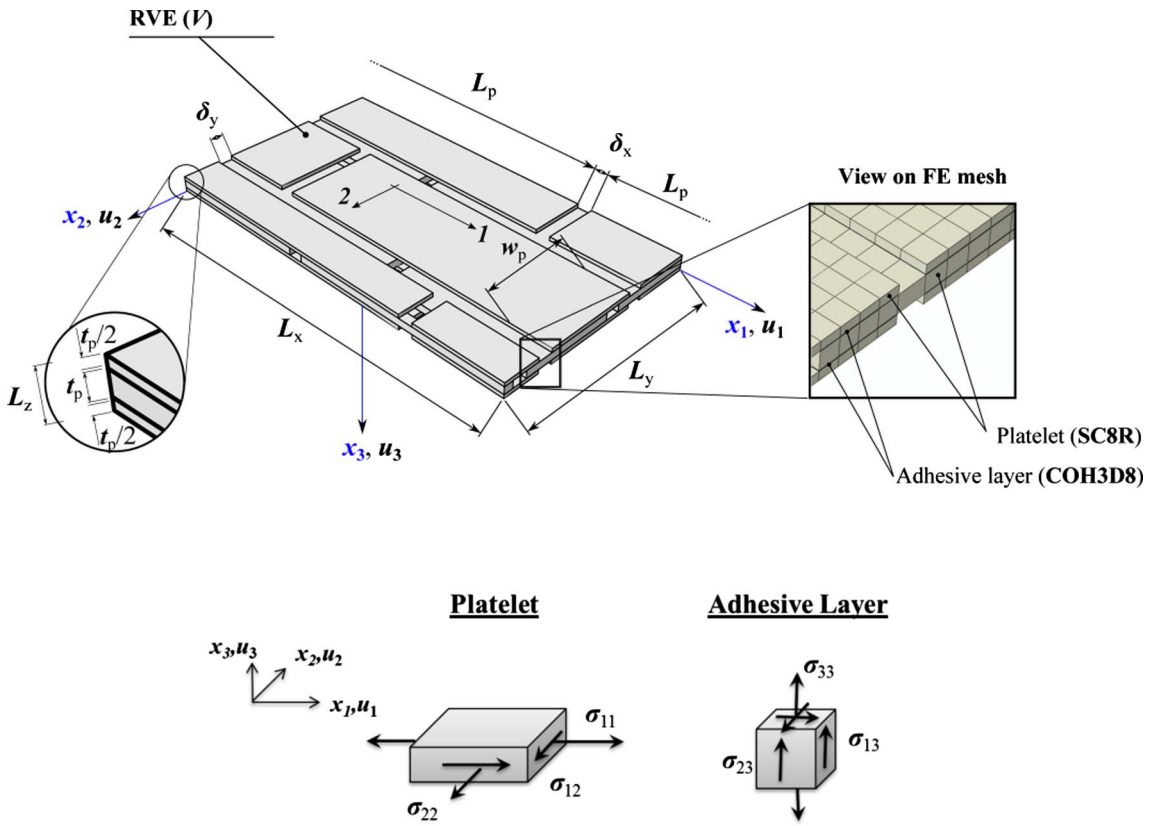

Fig. 2. RVE of a unidirectional array of precisely staggered platelets with schematics of idealized stress-carrying capacity of a platelet and resin layer (adhesive) between the platelets. (For interpretation of the references to colour in this figure legend, the reader is referred to the web version of this article.)

Table 1
Material properties of AS4/PEEK UD tape (from [43]).

Material properties	AS4/PEEK
Longitudinal modulus, E_{11} [GPa]	138
Transverse modulus, E_{22} [GPa]	10.2
Shear modulus, G_{12} [GPa]	5.7
Shear modulus, G_{23} [GPa]	3.7
Poisson's ratios, ν_{12}	0.3
Poisson's ratio, ν_{23}	0.45
Longitudinal tensile strength, X_t [MPa]	2070
Longitudinal compressive strength, X_c [MPa]	1360
Transverse tensile strength, Y_t [MPa]	86
Transverse compressive strength, Y_c [MPa]	230
Longitudinal shear strength, $S_{12} = S_{13}$ [MPa]	186
Transverse shear strength, S_{23} [MPa]	86

Table 2
Fracture properties of AS4/PEEK (from [44]).

Material properties	AS4/PEEK
Mode I delamination fracture toughness, G_{IC} [kJ/m^2]	1.7
Mode II delamination fracture toughness, G_{IIC} [kJ/m^2]	2.0

work was adopted from Matzenmiller et al. [48], who simplified the general anisotropic form to the symmetric form of Eq. (2). PFA is a combination of the failure criteria (damage initiation) and post-failure degradation rules at a local point in a heterogeneous material structure. The initiation of damage is governed by the effective stress components $\hat{\sigma}_{ij}$ through Hashin's criteria [49] shown in Eq. (3):

$$\text{Fiber tension} \quad (\hat{\sigma}_{11} > 0): \left(\frac{\hat{\sigma}_{11}}{X^T}\right)^2 = 1 \tag{3a}$$

$$\text{Fiber compression} \quad (\hat{\sigma}_{11} < 0): \left(\frac{\hat{\sigma}_{11}}{X^C}\right)^2 = 1 \tag{3b}$$

$$\text{Transverse tension} \quad (\hat{\sigma}_{22} > 0): \left(\frac{\hat{\sigma}_{22}}{Y^T}\right)^2 + \left(\frac{\hat{\sigma}_{12}}{S_{12}}\right)^2 = 1 \tag{3c}$$

$$\text{Transverse compression} \quad (\hat{\sigma}_{22} < 0): \left(\frac{\hat{\sigma}_{22}}{2S_{23}}\right)^2 + \left[\left(\frac{Y^C}{2S_{23}}\right)^2 - 1\right]\frac{\hat{\sigma}_{22}}{Y^C} + \left(\frac{\hat{\sigma}_{12}}{S_{12}}\right)^2 = 1 \tag{3d}$$

The material constants for Eq. (3) are given in Table 1. After the failure has been initiated by satisfying the given failure criteria, the corresponding stresses are degraded following a linear softening law. The evolution of damage is defined in terms of the fracture energy dissipated during the damage process [50], G_C. Some recommendations to determine these fracture energies can be found in [51,52]. In the present investigation numerical values for G_c were adopted from [36]. The longitudinal tensile and compressive fracture energy was assumed 12.5 kJ/m^2, while the transverse tensile and compressive fracture energy was taken as 1 kJ/m^2. The viscous regularization method [46,53], implemented in ABAQUS/Standard, was used to reduce damage localization and improve convergence. The strain rate dependence was introduced into the evolution law of a damage variable, d, as formulated in Eq. (4):

$$\frac{d}{dt}(d^v) = \dot{d}^v = \frac{1}{\eta}(d - d^v) \tag{4}$$

where η is a viscosity coefficient and d^v is the viscous (regularized) damage replacing the damage variable, d, in the constitutive equations. In the present work, the following stabilizing parameters were used for the damage model of a platelet: viscosity coefficient for the damage variable d_{11}, $\eta = 1(10^{-3})1/s$; viscosity coefficients for the damage variable d_{22}, $\eta = 5(10^{-3})1/s$. These numbers were adopted from [36].

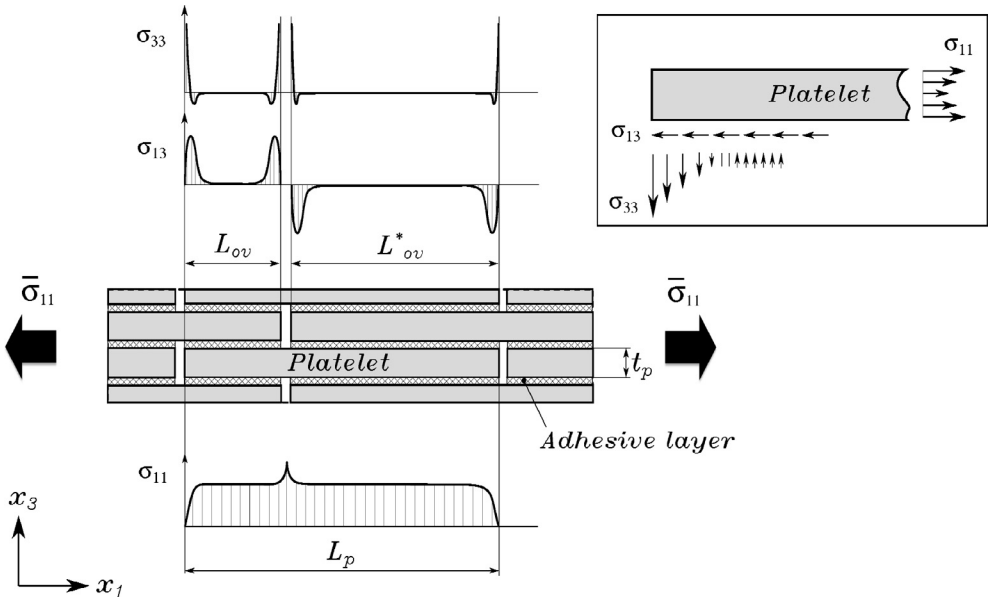

Fig. 3. Schematics of basic stress sharing in a platelet-arrayed composite system under uniaxial loading.

2.3.2. Damaged response of a platelet-to-platelet interface

Delamination of platelets was idealized with an interfacial damage model. Cohesive elements describe the evolution of the entire fracture process, from no crack to complete structural failure [35]. The interfacial (cohesive) element is characterized by a constitutive equation called a traction-separation law, which relates the interlaminar stress components, σ_{i3}, to the relative separations, $\delta_i = \Delta u_i$ ($i = \overline{1,3}$), between the top and bottom surfaces of the element:

$$\begin{Bmatrix}\sigma_{13}\\ \sigma_{23}\\ \sigma_{33}\end{Bmatrix} = \begin{bmatrix}(1-d)k_1^0 & 0 & 0\\ 0 & (1-d)k_2^0 & 0\\ 0 & 0 & (1-d)k_3^0\end{bmatrix}\begin{Bmatrix}\delta_1\\ \delta_2\\ \delta_3\end{Bmatrix} \tag{5}$$

In Eq. (5), $k_i^0 = 1(10^6)\text{Ł}\frac{\text{MPa}}{\text{mm}}$ ($i = 1-3$) is the initial stiffness and d is the isotropic damage variable which is a function of a single state variable, an effective displacement jump, δ_{ef}, to account for the mode-mixity:

$$\delta_{ef} = \sqrt{\delta_1^2 + \delta_2^2 + \delta_3^2} \tag{6}$$

The isotropic damage variable, d, is related to the effective displacement, δ_{ef}, by an assumed material softening law. The linear softening law for damage variable was adopted herein:

$$d = d(\delta_{ef}) = \frac{\delta_{ef}^f(\delta_{ef}-\delta_{ef}^0)}{\delta_{ef}(\delta_{ef}^f-\delta_{ef}^0)} \tag{7}$$

Prior to damage initiation ($\delta_{ef} < \delta_{ef}^0$) the value of d is equal to zero. After the damage initiation criterion is met ($\delta_{ef} > \delta_{ef}^0$), the tractions transmitted through the interface decrease with increasing opening (δ_3), sliding (δ_1) and tearing (δ_2) between adjacent platelets until a critical value of effective displacement jump, δ_{ef}^f, is reached. When $\delta_{ef} = \delta_{ef}^f$, the damage variable equals to one ($d = 1$), and the platelets are completely separated (interface fails). The damage initiation is controlled by a criterion which defines the corresponding effective displacement, δ_{ef}^0. The magnitude of the effective displacement jump at failure, δ_{ef}^f, is defined by the adopted delamination propagation criterion. A stress-based quadratic criterion was selected [54] for the initiation of disbonding between platelets, Eq. (8):

$$\left(\frac{\sigma_{33}}{N_{max}}\right)^2 + \left(\frac{\sigma_{13}}{S_{max}}\right)^2 + \left(\frac{\sigma_{23}}{T_{max}}\right)^2 = 1 \tag{8}$$

The numerical values of cohesive strengths used in the simulations were: $N_{\max} = 50$ MPa, $S_{\max} = T_{\max} = 70$ MPa. The expression for the effective displacement at damage initiation, δ_{ef}^0, corresponding to the quadratic criterion in Eq. (8) can be found in [37]. For the propagation of delamination, a linear fracture mechanics-based criterion was used [55]:

$$\frac{G_I}{G_{IC}} + \frac{G_{II}}{G_{IIC}} + \frac{G_{III}}{G_{IIIC}} = 1 \tag{9}$$

where G_{I}, G_{II}, and G_{III} are the work done by the tractions and their corresponding displacements in the normal and shear directions, respectively. Quantities with subscript "C" denote the critical strain energy release rates corresponding to each fracture mode (Table 2, assuming $G_{IIC} = G_{IIIC}$). The explicit form of the critical effective displacement at failure, δ_{ef}^f, defined by Eq. (9) can be found in [37]. Viscous regularization to improve the numerical convergence was used with viscosity coefficient of $\eta = 2(10^{-4})1/\text{s}$.

3. Uniaxial tension/compression of a unidirectional array of platelets

Progressive failure analysis was used as a tool to study the uniaxial strength of an array of aligned platelets under the prescribed macroscopic strain, $\bar{\epsilon}_{11}$. The effective/macroscopic response of the platelet meso-structure described in the previous section was calculated by computational homogenization wherein the macro-stress $\bar{\sigma}_{11}$ and strain $\bar{\epsilon}_{11}$ are the average of respective field stress and strains over the RVE volume, V, as shown in Eq. (10).

$$\bar{\sigma}_{11} = \frac{1}{V}\int_V \sigma_{11}(x_1,x_2,x_3)dV\,, \epsilon_{11} = \frac{1}{V}\int_V \epsilon_{11}(x_1,x_2,x_3)dV, \boldsymbol{x} \in V \tag{10}$$

3.1. Macroscopic stress-strain response of a platelet-array under uniaxial loading

The "shear-lag" type load transfer between the neighboring platelets governs the effective mechanical response of the platelet-arrayed composite system subjected to tension or compression. A platelet builds up an in-plane axial stress, σ_{11}, through the interlaminar shear and normal (peel) stresses acting over its interfaces (see Fig. 3). The interfacial shear stress is the primary mechanism to equilibrate the in-plane normal stresses in the platelet. The interfacial shear stresses, σ_{13} and σ_{23}, are concentrated near the periphery of platelet-to-platelet overlap regions with their greatest values near the edges of the platelet and then decrease rapidly to a near-zero value towards the mid-length of the

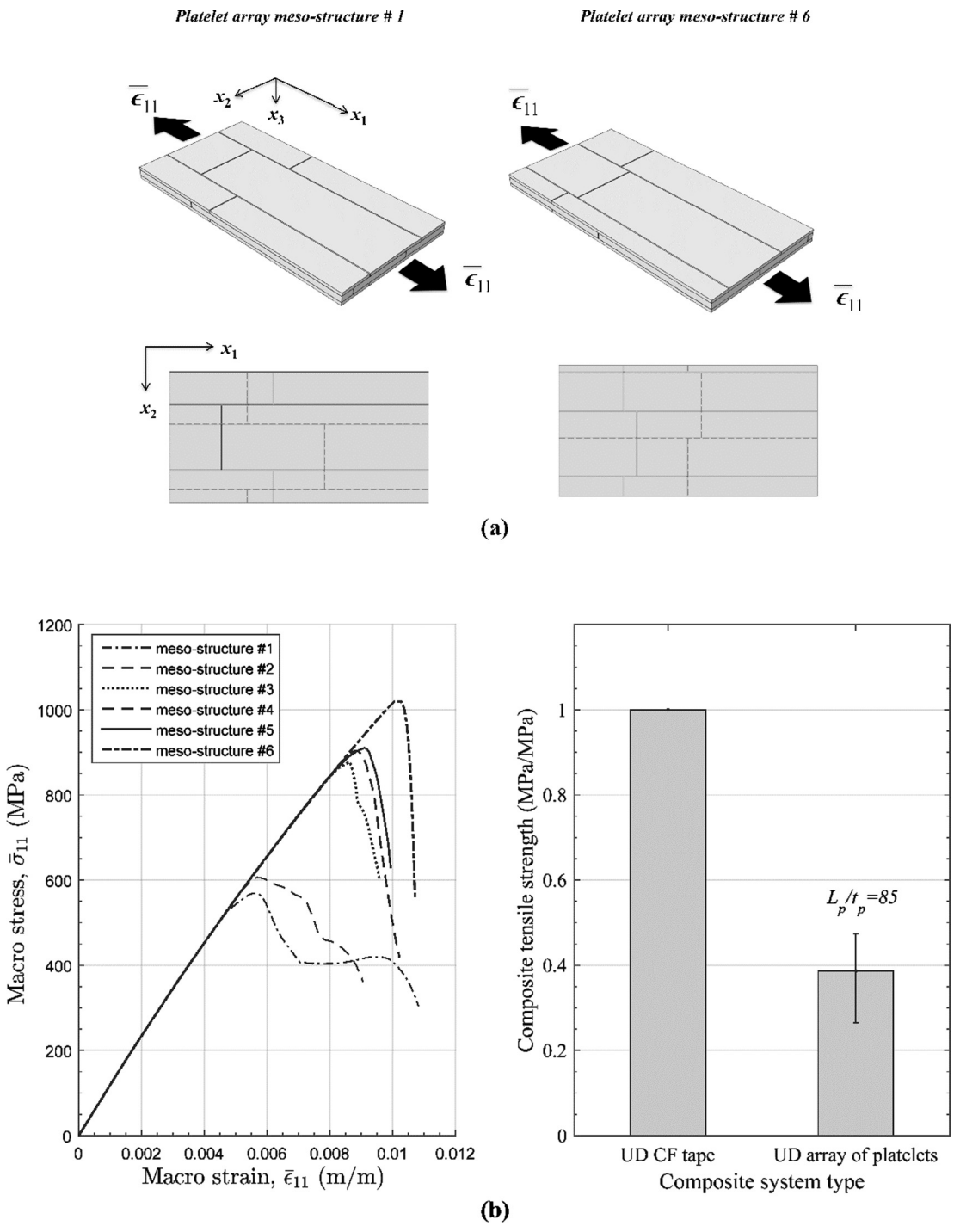

Fig. 4. (a) Two sample meso-structures (morphologies) of a UD-arrayed platelet composite system; (b) Homogenized stress-strain curves of several UD-arrayed composites with various morphologies under uniaxial tensile loading (left), and reduction of platelet-composite effective strength from the parent CF UD tape strength (right), L_p/t_p = 85.

overlap. The interfacial normal stress, σ_{33}, is induced by the eccentricity in the load path. It peaks at the edge of a platelet-to-platelet overlap and decays rapidly away from the edge. The in-plane normal stress in a platelet, σ_{11}, declines near the platelet edges and vanishes at the platelet edge. The axial normal stress in a platelet peaks at the discontinuity of adjacent platelets. This extra stress results from the adjacent platelets unloading their normal stresses.

The axial strength of the platelet meso-structure is determined by the two interacting mechanisms described earlier. When the geometry of the meso-structure is chosen such that interlaminar failure is retarded, tensile failure of the platelet controls failure of the meso-structure. The second mechanism is illustrated when the interlaminar failure of the meso-structure occurs at platelet tensile stresses significantly less than its tensile strength. Thus, meso-structures corresponding to the tensile failure of the platelet can be characterized as an efficient load transfer geometry, while the latter geometry is deemed inefficient.

The macro stress-strain curve of a meso-structure under axial loading exhibits several stages. Prior to damage initiation, the effective stress-strain response is linear-elastic. After damage initiation, the platelet meso-structure starts developing the damage process zone (DPZ), which is an accumulation of growing and coalescing damaged

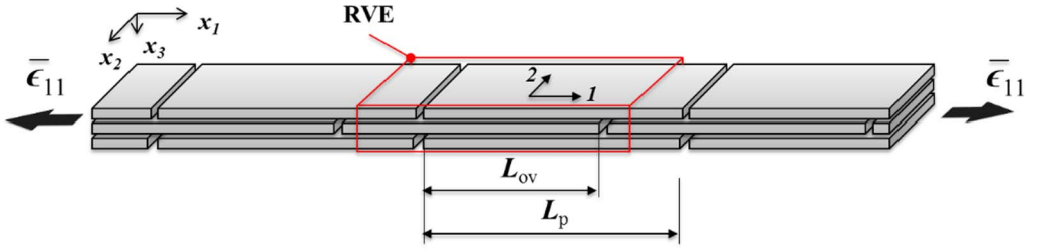

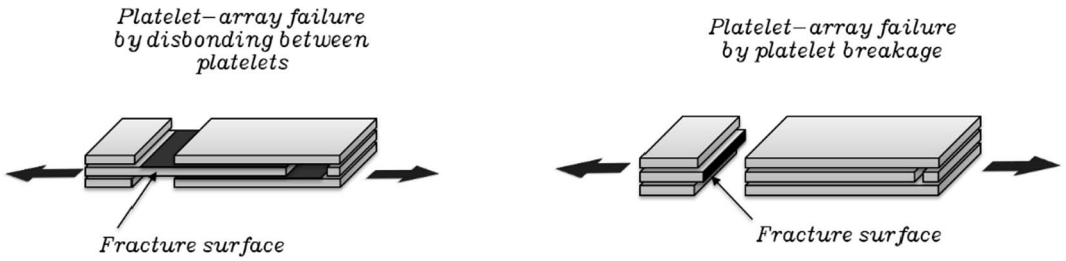

$$\left[1-\left(\frac{L_{ov}}{L_p}\right)_{cr}\right] < \frac{L_{ov}}{L_p} < \left(\frac{L_{ov}}{L_p}\right)_{cr} \qquad \left[1-\left(\frac{L_{ov}}{L_p}\right)_{cr}\right] \geq \frac{L_{ov}}{L_p} \geq \left(\frac{L_{ov}}{L_p}\right)_{cr}$$

(a)

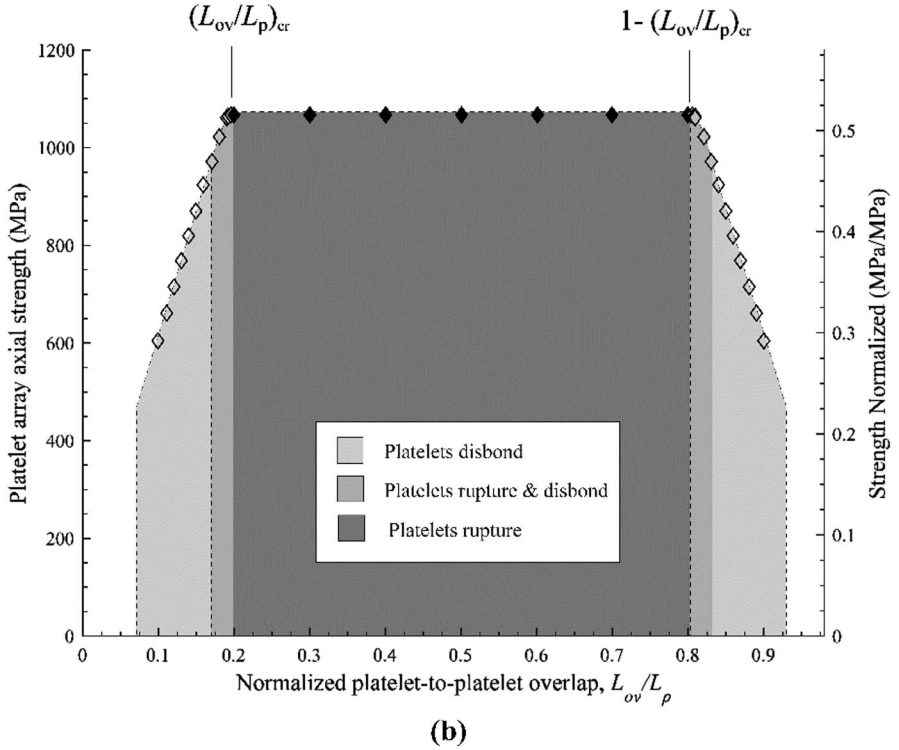

(b)

Fig. 5. (a) RVE to study the effect of overlap length between platelets with schematics of possible failure modes; (b) UD platelet array strength versus overlap length-to-platelet length fraction (L_p/t_p = 85). (For interpretation of the references to colour in this figure legend, the reader is referred to the web version of this article.)

local regions. With the incipience of the DPZ, the platelet meso-structure stress-strain relationship exhibits non-linear behavior, termed strain hardening:

$$\bar{\sigma}_{11} = \bar{C}_{11}(\bar{\epsilon}_{11})\bar{\epsilon}_{11} \tag{11}$$

where the effective stiffness, $\bar{C}_{11}(\bar{\epsilon}_{11})$, changes with the applied strain, $\bar{\epsilon}_{11}$, as the meso-structure accumulates damage and DPZ grows. The first damage that occurs requires lower energy consumption. The localized delaminations near platelet edges happen early in the loading history due to stress concentrations near the platelet ends. As the applied load is increased, the interfacial delamination grows. The extent of the interfacial fracture process zone growth depends on the both the meso-

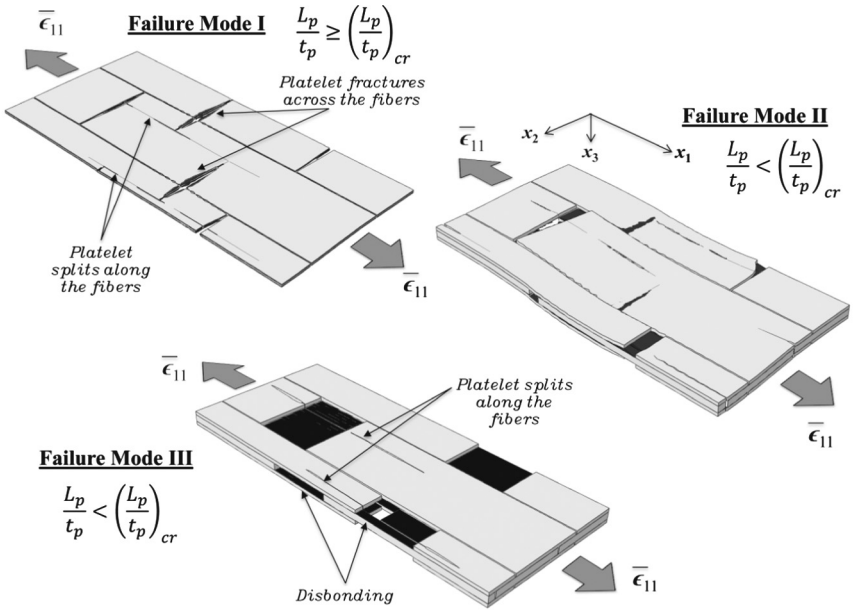

(a)

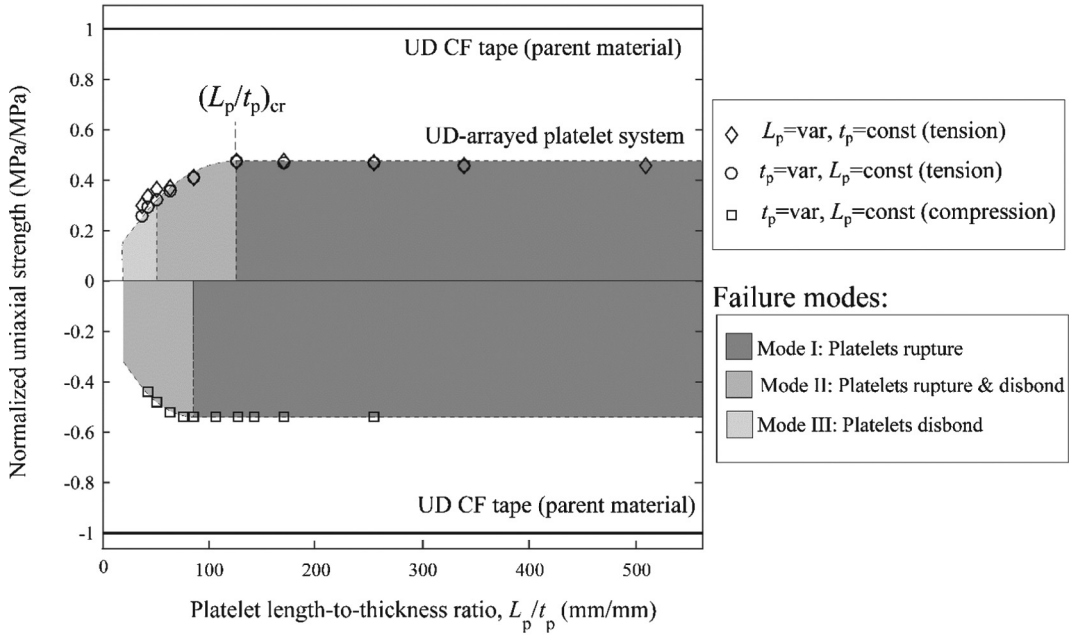

(b)

Fig. 6. (a) Possible failure modes (sketch from simulated results) for a given composite morphology; (b) variation of tensile/compressive strength of a platelet-arrayed composite system with platelet length-to-thickness ratio, L_p/t_p (normalized by the corresponding uniaxial strength of the parent UD CF tape); the map of failure type is also shown; (c) variation of effective tensile response of a platelet-arrayed composite system with platelet length, L_p, and thickness, t_p.

structure and platelet geometries. The interfacial facture process zone is highly localized for large platelet length to thickness ratio and overlaps of substantial length, but can consume the entire interface when meso-structures produce largely interlaminar damage for low platelet length-to-thickness ratio. Eventually, the fully developed DPZ translates into a macroscopic crack, which leads to the ultimate failure of the entire meso-structure since the system can no longer support an increase in the applied load. The size and type of a DPZ is a property of the meso-structure and platelet strength properties. The macroscopic crack can have a complex topology appropriate to a particular failure mode of the system including the splits in the fiber direction and fractures perpendicular to the fiber direction in the platelets, delamination between platelets and combinations of the three. The topology of the macro-crack is thus related to the attainable strength value of the composite. The more diffused DPZ (with more interfacial damage) results in a lower energy consumption to ultimate failure and, consequently, a lower effective strength of the meso-structure. The more localized DPZ would involve platelet fiber breakage on the last stages of damage and require more significant energy input. When the size of DPZ is relatively small compared to RVE-size, the composite typically exhibited a more

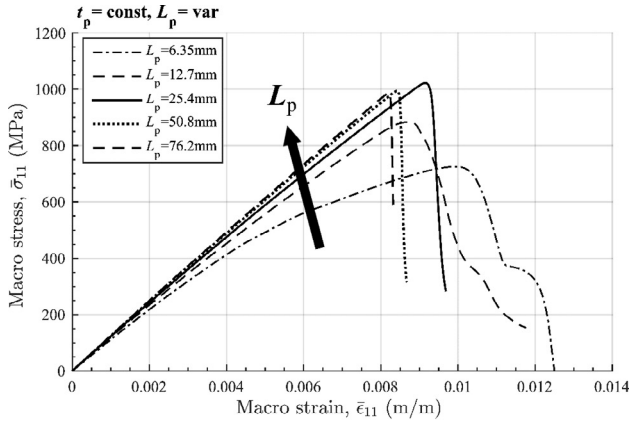

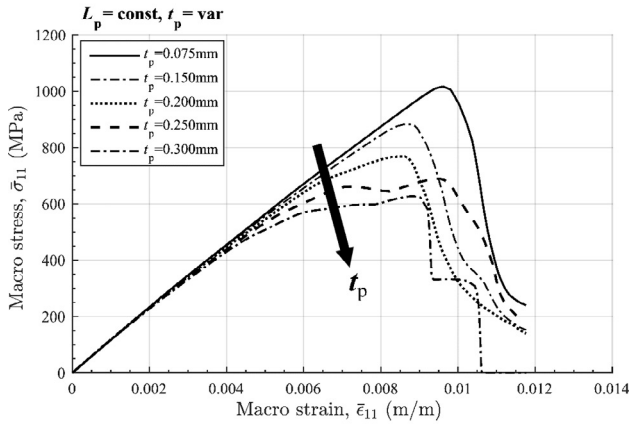

(c)

Fig. 6. (*continued*)

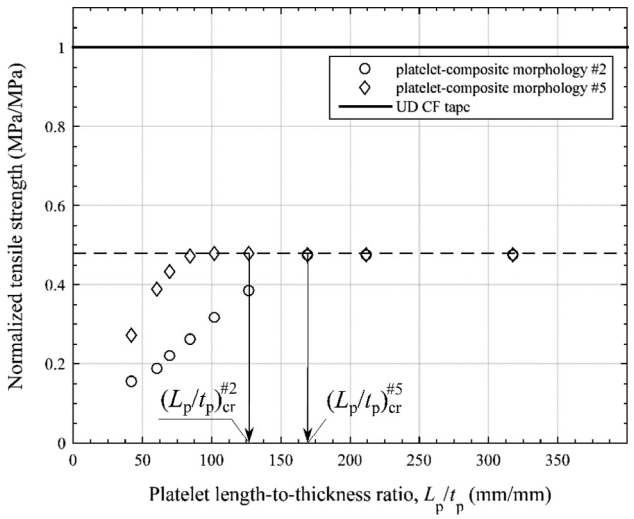

Fig. 7. Composite morphology dependence of a platelet critical length-to-thickness aspect ratio, $(L_p/t_p)_{cr}$.

brittle response. If the DPZ encompasses a significant portion of RVE, the more ductile effective response is observed.

In the following sections the effective strength of a platelet-arrayed composite and its failure mode are shown to be determined by (i) the composite morphology, and (ii) the length-to-thickness ratio of the platelet.

3.2. Effect of meso-structure geometry on system tensile strength

An array of aligned platelets can exhibit substantially different strengths and failure modes depending on the local heterogeneity (meso-structure morphology) defined by the spatial arrangement of platelets. The overlap length was found to play an essential role in the load transfer mechanism. Increasing the overlap length between platelets increases the tensile stress carried by the platelets and improves the effective strength of the composite system to the limiting magnitude.

The developed RVE-based computational model was first exercised to study the variation in tensile response of a meso-structure as a function of its morphology. Several RVE architectures were generated (see Appendix A) with various geometric arrangements of platelets in both planar (x_1x_2) directions, while holding the platelet volume fraction constant. Herein, the following geometrical parameters were used: L_p = 12.7 mm, $L_p/w_p = 4$, t_p = 0.150 mm, δ_x=-= δ_y = 50 μm, t_{coh} = 5 μm. Fig. 4(a) shows an example of the two different RVE geometries of a platelet meso-structure. Fig. 4(b) shows the homogenized stress, $\bar{\sigma}_{11}$, to failure as a function of the applied uniaxial tensile strain, $\bar{\epsilon}_{11}$, for several platelet meso-structures. E.g., meso-structure #6 had the longest and the most uniform overlap areas sufficient for the platelets fiber fracture, thus exhibiting the greatest macroscopic (effective) strength, which made about half of the platelet longitudinal strength. The considered type of morphology determines the composite limiting strength. When a platelet is sandwiched between the matching discontinuities, the composite net cross-sectional area is a half of the composite gross cross-section area. Therefore, even when a platelet can take enough stress for fibers fracture, the composite strength is around one-half of the longitudinal strength of a platelet. Stress-strain curves in Fig. 4(b) show that the composite performance can be substantially enhanced or depressed just by modifying the overlap lengths between platelets. A summary of the meso-structure tensile strengths (average along with predicted variation) as compared to the prepreg fiber-direction strength is shown in Fig. 4(b).

The overlap length of adjacent platelets is seen to be an important parameter for determining the strength of a platelet meso-structure. For this reason, a simplified geometry, shown in Fig. 5(a), with a single platelet in the x_2-direction was considered to systematically study the effect of the overlap length between platelets, L_{ov}, on the meso-structure tensile strength. The results are shown in Fig. 5(b) where the strength is shown versus the overlap length normalized by the platelet length, L_{ov}/L_p. The platelet length and thickness used in the analysis were L_p = 12.7 mm and t_p = 0.15 mm. For a given platelet geometry, the meso-structure strength increases almost in proportion to the overlap length for small values, but becomes insensitive to the overlap length for larger overlap length. The maximum achievable strength (under the assumed arrangement of platelet layers) corresponded to the L_{ov}/L_p ratio greater than 0.2. The strength achieved was approximately 50% of that of the parent material (UD tape) strength and is the result of platelet fracture in the fiber direction. This result shows that there exists a critical overlap length between platelets (for a given arrangement of platelets) beyond which the platelets fail and, consequently, exhibit their full potential. When a platelet overlap length is below the critical value, the stress sharing between platelets is insufficient to fracture a platelet. The composite strength is then reduced by the change in failure mode with platelets disbonding from one another due to enhanced interfacial stresses. The failure modes of the two meso-structures are shown in Fig. 5(a): the dis-bonding between platelets (or platelet pull-out) where fracture surface is in the platelet-to-platelet interface, and the platelet fracture under intact interface (fracture surface passes through the platelet).

3.3. Significance of platelet length-to-thickness ratio on tensile/compressive strength

The platelet length-to-thickness aspect ratio, L_p/t_p, is shown to have a strong effect on the effective tensile/compressive properties of a given meso-structure. A greater aspect ratio improves the efficiency of the stress transfer and thus increases effective strength of a composite

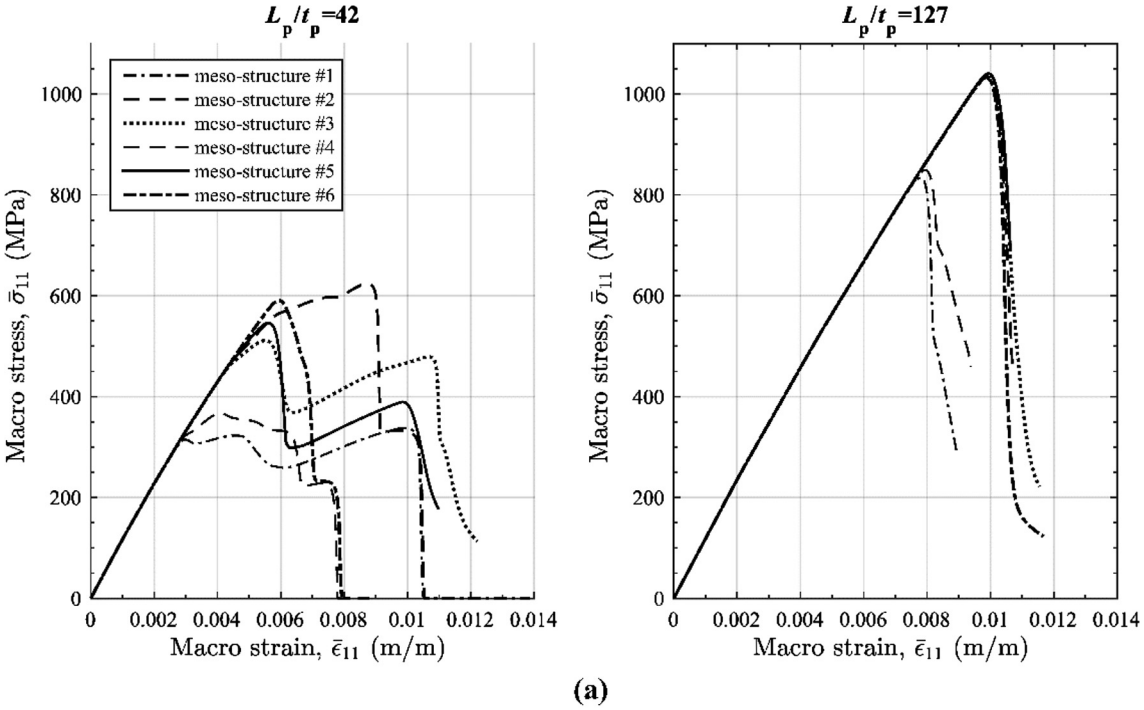

(a)

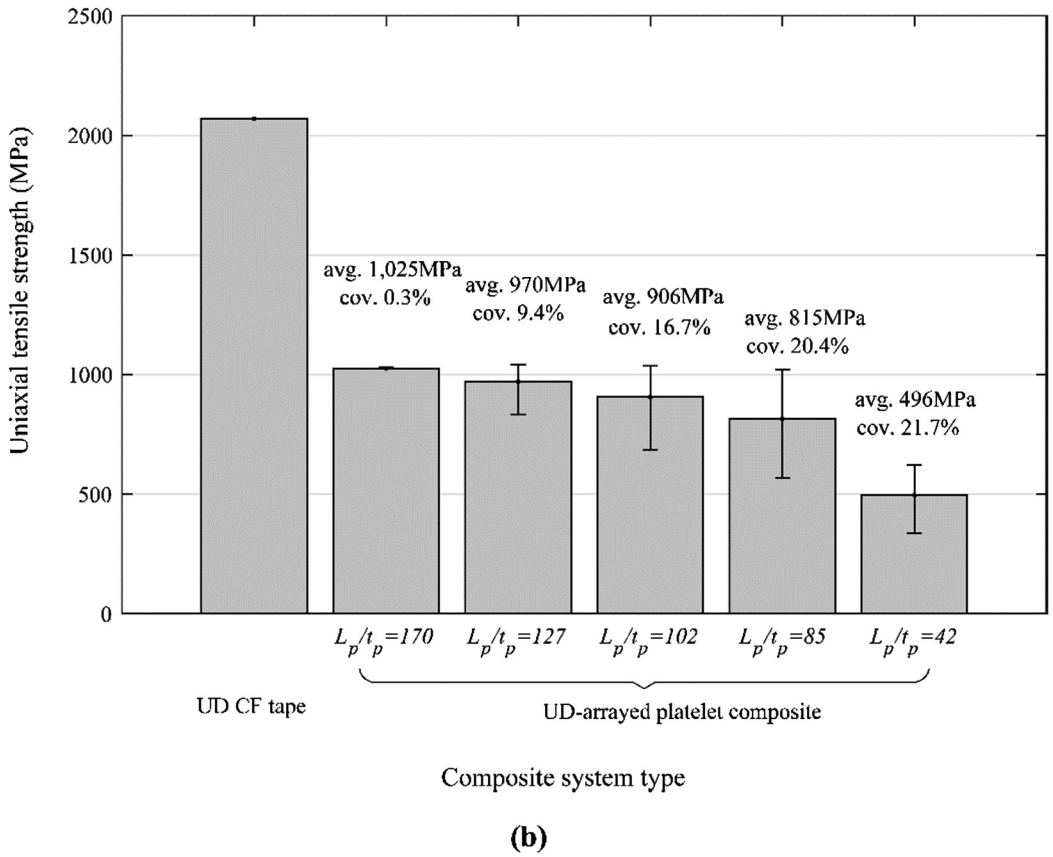

(b)

Fig. 8. (a) Development of morphology independence of effective composite tensile response with increased platelet (L_p/t_p)-ratio; (b) mitigation of morphology caused variation of tensile strength with increased platelet L_p/t_p-ratio in a UD-arrayed platelet composite system.

system by shifting the dominant damage mode from platelet delamination (pullout) to platelet longitudinal tensile fracture.

The effect of a platelet length and thickness was investigated independently first in a meso-structure with a given morphology ($L_p/w_p = 4$). First, the platelet thickness, t_p, was kept constant at 0.150 mm with platelet length varying in range of L_p = (6.35…76.2) mm. Next, the platelet length, L_p, was kept constant at 12.7 mm with platelet thickness varying in range of t_p = (0.075…0.3) mm. Fig. 6(a) shows the

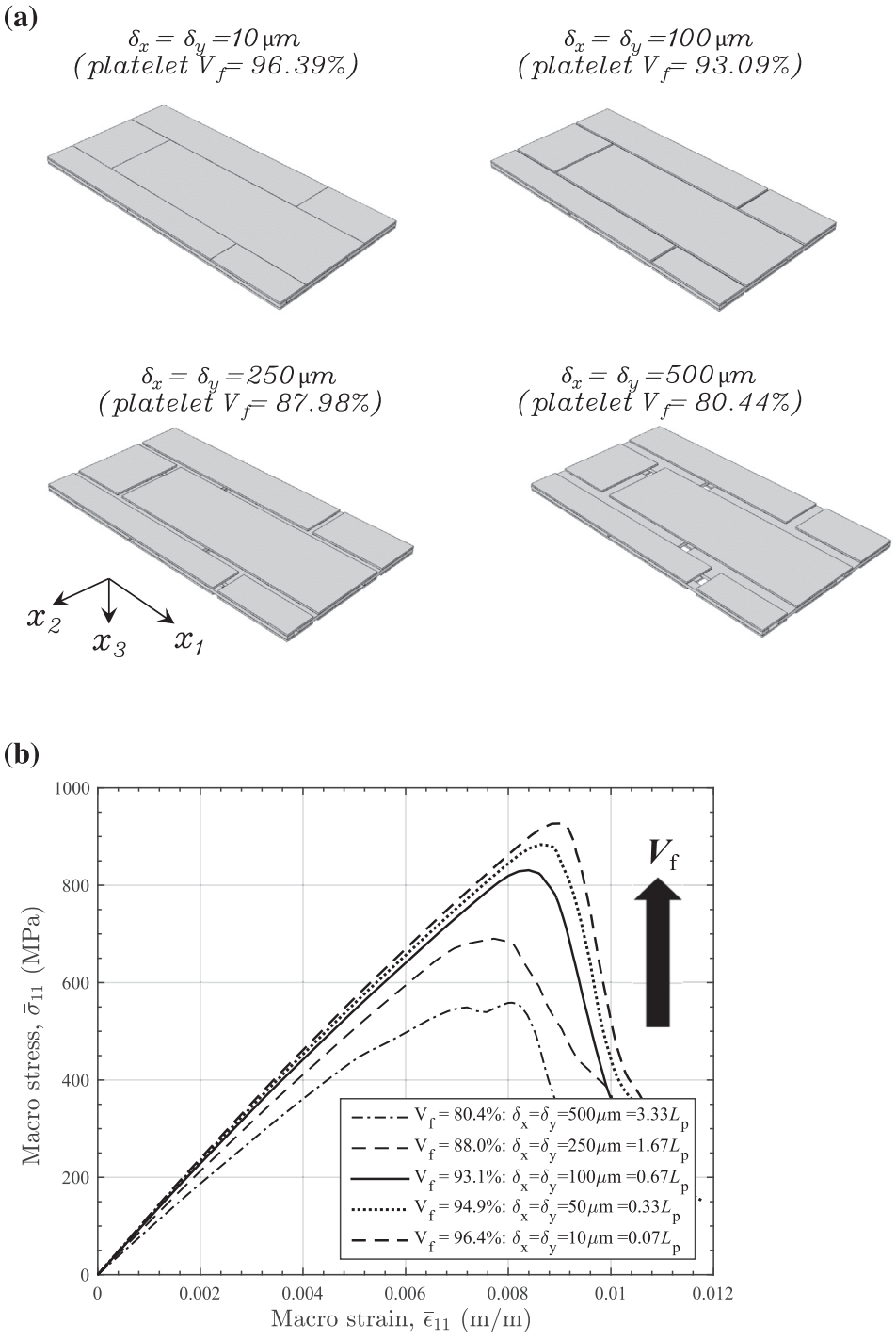

Fig. 9. Tensile response of a UD-arrayed platelet system as a function of platelet volume fraction: (a) variation of platelet volume fraction by changing the spacing between platelets; (b) effective stress-strain curves of a composite for different platelet volume fractions.

topologies of the simulated macro-cracks corresponding to the distinctly different failure modes of the meso-structure by varying the platelet aspect ratio. Fig. 6(b) summarizes the effective strength data from the homogenized stress-strain curves for the array of platelets with t_p = var (L_p = const) and L_p = var (t_p = const) shown in Fig. 6(c). The parent material (UD CF tape) longitudinal strength normalizes the meso-structure strength in Fig. 6(b). From data in Fig. 6(b), the arrays with platelets of different length and thickness, but with the same L_p/t_p-ratio exhibit the same effective strength. Thus, a platelet length-to-thickness, L_p/t_p, aspect ratio is shown to be a governing factor. When a platelet length is small and its thickness is large (the platelet length-to-thickness ratio is sufficiently small) the inefficient stress sharing between platelets depresses the composite effective strength since the composite fracture occurs largely through platelet-to-platelet interface which is typically weaker than the platelet itself. The delamination is accompanied by transverse splits in platelets from stress concentrations at the edges of neighboring platelets, as shown in Fig. 6(a) denoted Failure Mode III. The increased platelet length-to-thickness ratio shifts the damage distribution from the interface into the platelet itself. The high aspect ratio platelets tend to fracture across the platelet and split parallel to the fiber direction, where they are confined between the matching junctions between the platelets above and below. By

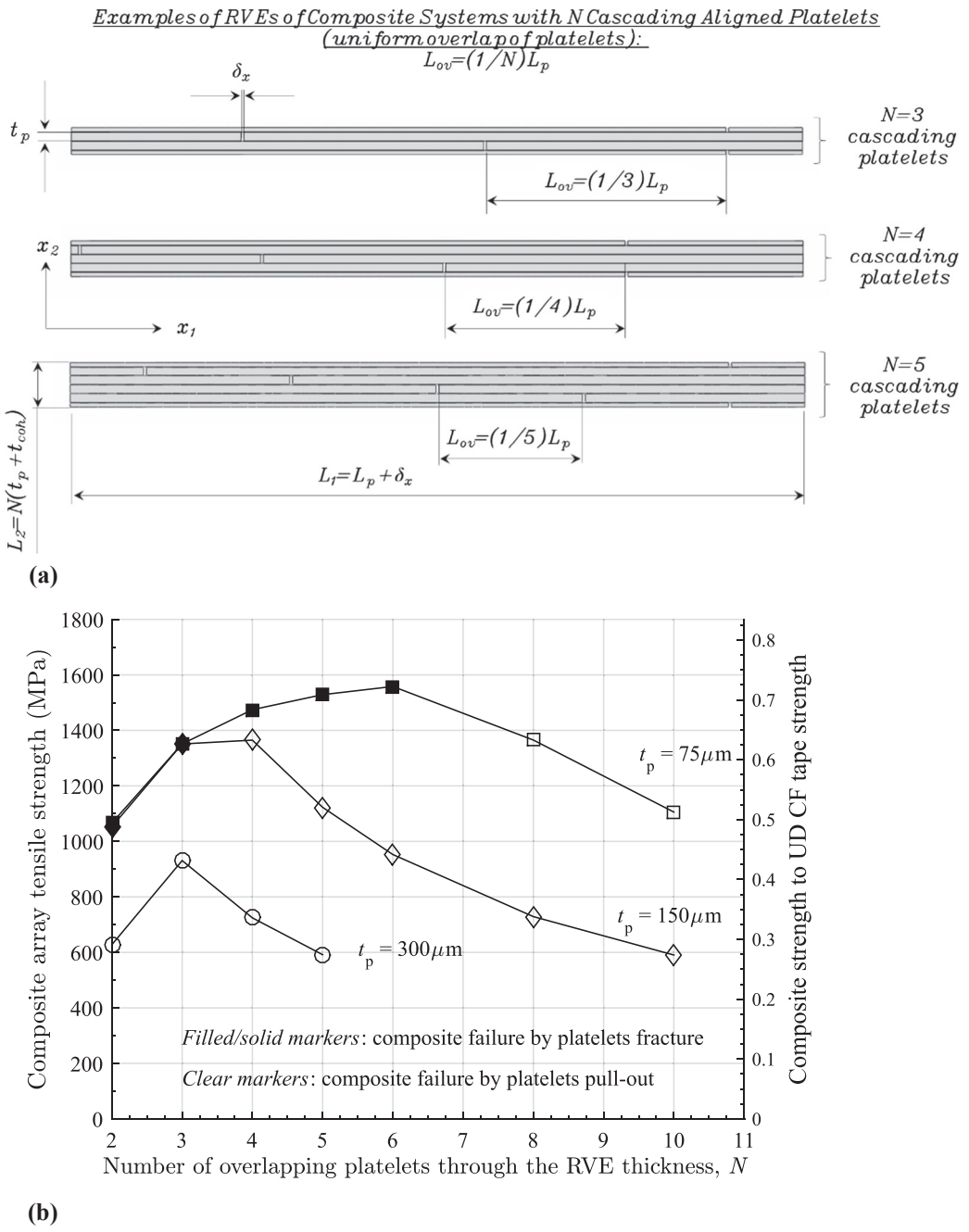

Fig. 10. Effect of added redundancy on uniaxial tensile strength in array of cascading and uniformly overlapping platelets (L_p = 12.7 mm, L_p/w_p = 4): (a) schematics of composite system morphology; (b) tensile strength as a function of composite structure (morphology and platelet geometry).

maximizing platelet length-to-thickness aspect ratio, the dis-bonding effects of platelets through the interface can be reduced, so that the composite strength is increased, see Failure Modes I and II in Fig. 6(a) and (b).

The results in Fig. 6(b) allow one to estimate the critical platelet aspect ratio as 125 in tension and 75 in compression for a given meso-structure. Platelet critical length-to-thickness aspect ratio is the ratio below which the platelet does not experience complete tensile fracture in the fiber direction.

3.4. Platelet length-to-thickness critical ratio as a function of meso-structure morphology

The concept of critical platelet length-to-thickness ratio is further complicated by the arrangement of overlaid platelets. The plateau-strength of a platelet-arrayed meso-structure is reached at the critical (L_p/t_p)-ratio of a platelet. However, different assumed morphologies will have different apparent critical aspect ratios, $(L_p/t_p)_{cr}$, as shown in Fig. 7. This can be explained by the influence of overlap length of adjacent platelets on the effectiveness of stress sharing within the meso-structure with a given morphology, suggesting that any array of platelets is a structural system in its own right. In other words, if there is a lot of overlap length, then there is no need for as much L_p/t_p-ratio to maximize the composite strength; inversely, a greater L_p/t_p-ratio will be required to compensate smaller overlap areas and suppress delaminations.

Generally, in solid mechanics, a critical parameter characterizes the bifurcation point between the distinct behavioral patterns of a system. The critical parameter always depends on the architecture of a structural system. Thus, the effective response of a meso-structure emerges

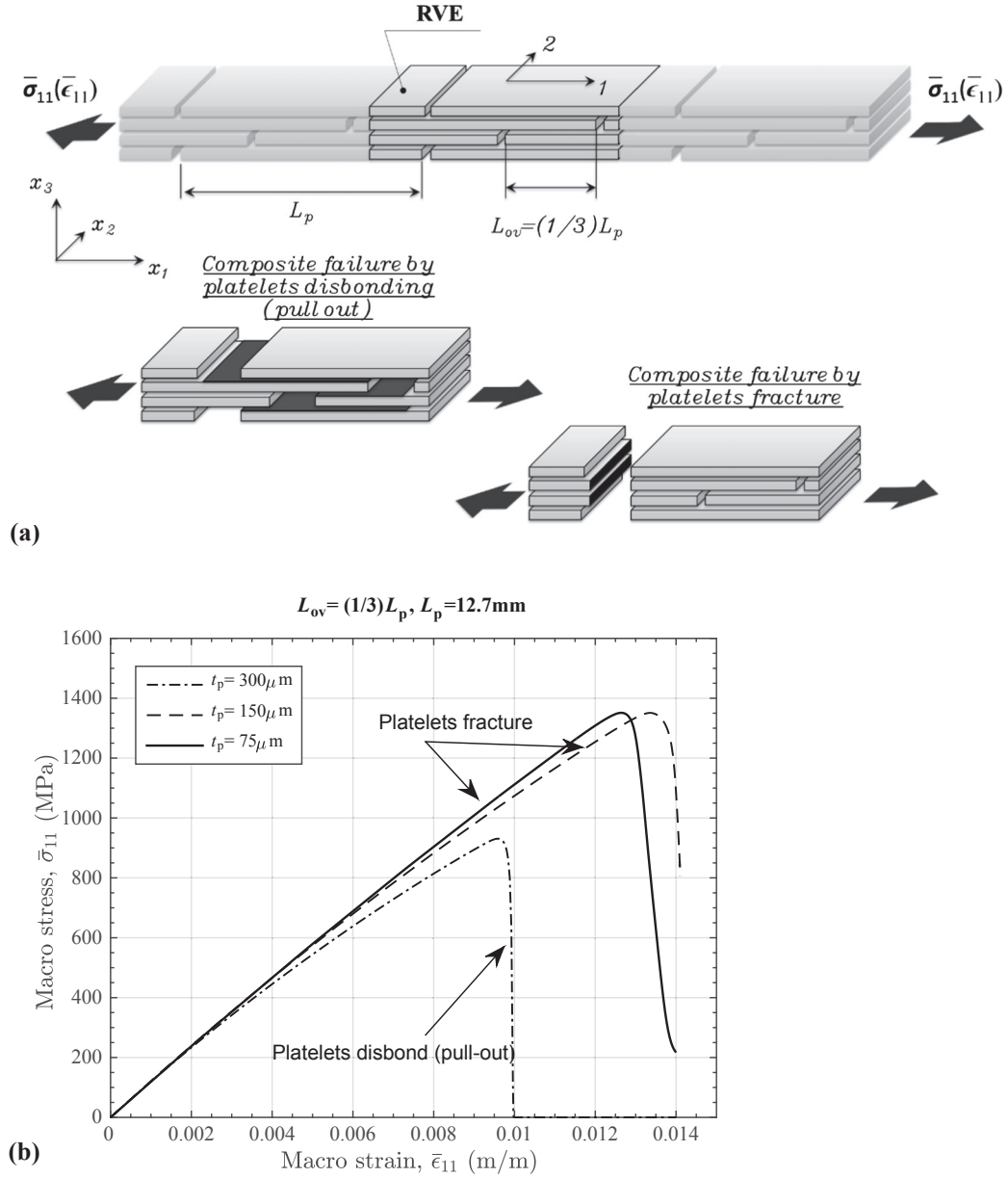

Fig. 11. (a) Failure modes in a composite array of three cascading platelets; (b) Effective response of a composite array with three cascading platelets as a function of platelet thickness.

from both the platelet characteristics and the platelet arrangement. The critical overlap length between platelets exists for the fixed platelet dimensions, but then, for a considered arrangement of platelets, there exists a critical geometrical configuration of an individual platelet. This reflects the dualism and inter-play between the platelet ("element") and the meso-structure ("system") that control the composite performance.

3.5. Mitigation of composite strength variability from morphology by increased platelet length-to-thickness ratio

When a platelet-arrayed meso-structure failure is dominated through the platelet-to-platelet interface such as for platelets of low L_p/t_p-ratio, the meso-structure morphology controls effective strength. Thus, variability in meso-structure is translated to variability in strength. As the dominant damage is moved into platelet tensile failure with $(L_p/t_p) \rightarrow (L_p/t_p)_{cr}$, the meso-structure arrangement becomes less important and the meso-structure strength becomes more morphology independent. That is, variability in meso-structure arrangement is not translated directly to its strength variability.

Thus, the mitigation of morphology-dependence of meso-structure strength can be achieved with increased platelet length-to-thickness ratio. This is illustrated by the data in Fig. 8(a) and (b), where the same morphologies used in Section 3.2 were investigated for their strength sensitivity to the platelet length-to-thickness ratio (L_p/t_p). It can be seen that the macro responses of the six meso-structures are very different from one another at L_p/t_p = 42, but as the platelet aspect ratio is increased to L_p/t_p = 127, the responses of meso-structures 1 and 2 become very close, while the macro stress-strain curves of meso-structures ## 3, 4, 5, 6 are essentially indistinguishable in graphics scale. A noticeable reduction of coefficient of variance (cov) and increased average (avg) strength result from the increased (L_p/t_p)-ratio, as it can be seen in Fig. 8(b).

3.6. Effect of platelet volume fraction on composite tensile strength

Platelet volume fraction, V_f, in an RVE is defined by the relationship given in Eq. (12):

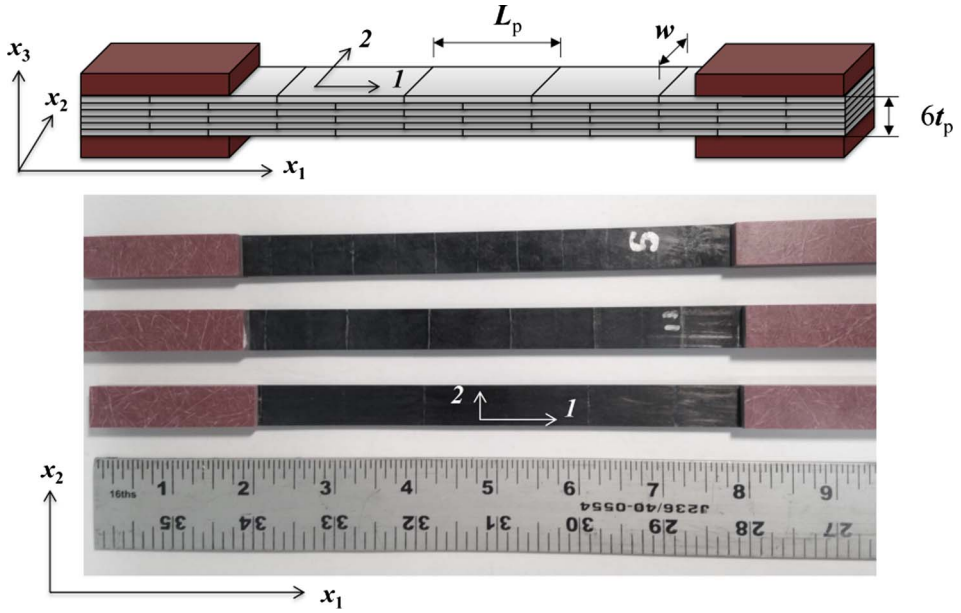

Fig. 12. Experimental tensile bars made of platelets to study the effect of L_p/t_p-ratio on effective strength (schematics on top and a photograph of several coupons on bottom). (For interpretation of the references to colour in this figure legend, the reader is referred to the web version of this article.)

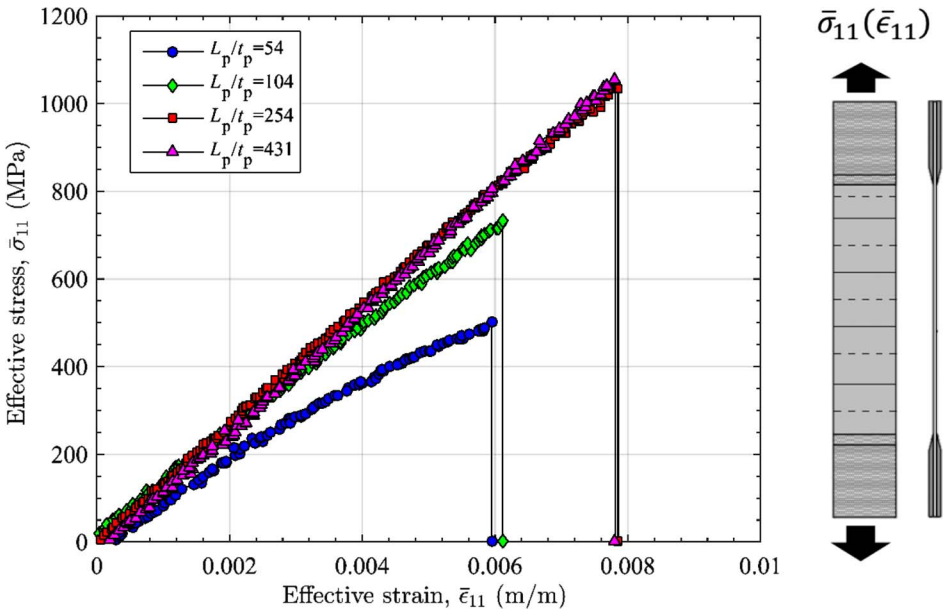

Fig. 13. Representative effective stress-strain curves (experimental) for various length-to-thickness ratio of a platelet. Herein, platelet thickness was constant (thickness of a single layer of a parent UD CF tape), and length was varied. (For interpretation of the references to colour in this figure legend, the reader is referred to the web version of this article.)

$$V_f = \frac{4 \cdot V_{platelet}}{V_{RVE}} = \frac{4 L_p w_p t_p}{L_x L_y L_z} \tag{12}$$

Platelet volume fraction is modified by varying the in-plane spacing between platelets ($\delta_x = \delta_y$), see Fig. 9(a). The stress-strain curves for UD-arrayed platelet systems with different platelet volume fractions are shown in Fig. 9(b). It can be seen that the stress-strain curves are linear in the initial stage of axial tension for all platelet volume fractions. The curves slope increases with increasing platelet volume content, meaning the composite system effective stiffness (tensile modulus) increases with increased platelet volume fraction. The curves slope begins to decrease when damage progresses through the system. The ultimate strength of the composite increases with increasing platelet volume fraction, as well as the ultimate (failure) strain. For a particular RVE meso-structure (#4), the variation of platelet volume fraction from 87.98% to 96.39% (increase by 10%) leads to the improvement of ultimate tensile stress from 690 MPa to 927 MPa (increase by 34%). The reported data corresponds to the platelet size of $L_p = 12.7$ mm, $t_p = 0.15$ mm, $L_p/w_p = 4$.

3.7. Effect of added redundancy on uniaxial tensile strength in array of cascading and uniformly overlapping platelets

Consider a periodic composite array of N platelets uniformly overlapping with one another in a cascading manner and aligned with the loading x_1-direction. The RVE of a composite has length in the x_1-direction (L_1) equal to the sum of platelet length and the gap between platelets, while the RVE height (L_2) is $N(t_p + t_{coh})$, as shown in Fig. 10(a) for several arrays having different number of cascading platelets. In such composite system, $(N - 1)$ platelets are sandwiched between the matching junctions of neighboring platelets in the

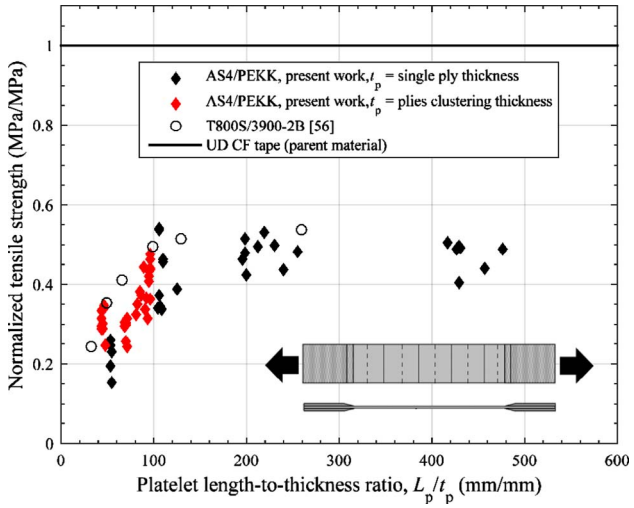

Fig. 14. Experimentally found dependence of effective tensile strength of platelet-arrayed coupons on a single platelet L_p/t_p-ratio. (For interpretation of the references to colour in this figure legend, the reader is referred to the web version of this article.)

composite through-thickness direction. This composite system has a more complex morphology as compared to the previously considered systems, with added redundancy from a greater number of platelets included into it. Structural redundancy plays many parts, for example in the behavior of the overall structure following some form of damage. Having more elements in the system, both platelets and interfaces, provides more paths for energy dissipation during the damage growth through the composite system. On the other hand, more platelets added to the system reduces the platelet-to-platelet overlap, therefore increasing the interfacial stresses. Besides, the platelet geometry is as before responsible to control the stress transfer within the system.

Added redundancy from an increased number of platelets in a system of cascading platelets can enhance the composite effective strength by redistributing the load-transfer between more elements. At some point though, a further increase in platelet count produces greater chances to have a morphology with a "week spot", meaning short and over-stressed platelet-to-platelet overlaps, such that effective composite strength would be suppressed. It is shown in Fig. 10(b) for several platelet thickness magnitudes. Both platelets fracture and platelets disbonding are possible, as shown in Fig. 11 for the case of a periodic system with three uniformly overlapping platelets. When the platelet-to-platelet interfacial damage is minimized, the composite effective strength is maximized. Contrary, when composite overall failure is through the disbonding between the platelets, the composite effective strength is retarded.

4. Experimental evidence of the platelet aspect ratio significance

Experimental work has been performed to study the effect of a platelet length-to-thickness ratio on the macro-response of a platelet meso-structure in terms of its effective strength and failure mode. Experimental results show the similar trends to the computational work of Section 3.3 and therefore support its conclusions.

Tensile coupons representing the arrays of aligned platelets (Fig. 12) were manufactured from the AS4/PEKK UD CF tape (Cytec/Solvay). Precursor UD prepreg was cut into the strips perpendicular to the fiber direction with the intervals of desired platelet length (L_p). The strips were 2 in. (50.8 mm), 1 in. (25.4 mm), 0.5 in. (12.7 mm), and 0.25 in. (6.35 mm). Then, the strips were stacked together to fabricate a staggered system of platelets, resulting in a flat plate/panel. The strips were slightly soldered together to maintain proper positioning during layup. The layers of release agent were applied to the mold surface. The platelet ensemble (a plate) was placed inside the mold cavity. The mold was closed and heated up in the oven, with a thermocouple probe inserted into it for temperature control. After reaching the melt temperature, the composite panel was molded in a press at about 200 psi (1.38 MPa). The material was held under pressure while cooling down in air at room temperature. The plate was next equipped with end tabs and cut to the specimen dimensions on the surface grinder. The tensile coupons were 10 in. (254 mm)-long (with about 6 in. (152 mm)-gage length) and 0.5 in. (12.7 mm)-wide. An MTS

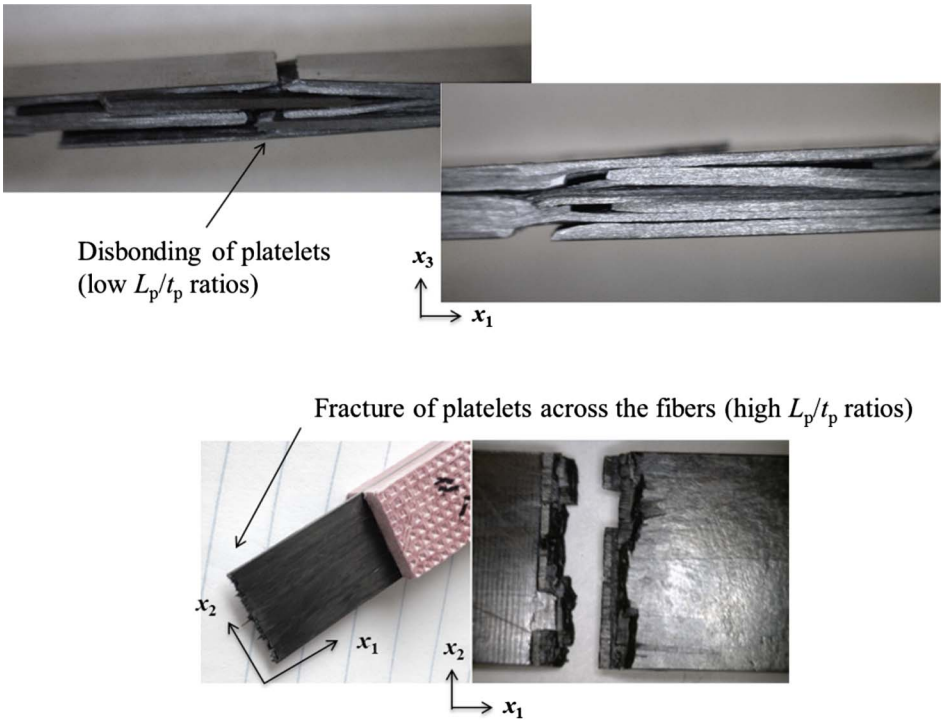

Fig. 15. Experimentally observed change of the failure type in platelet-arrayed tensile coupons: from dis-bonding dominated failure for the low platelet aspect ratios to the platelet fiber fracture dominated failure for the high aspect ratios. (For interpretation of the references to colour in this figure legend, the reader is referred to the web version of this article.)

machine with hydraulic grips and 22 kip (97.86 kN) load cell was used. The specimens were tested in tension with loading axis, x_1, parallel to the fiber direction of platelets. The displacement control with loading rate of 2 mm/min was used.

For the specimen geometry shown in Fig. 12, each coupon was produced with a single platelet across the width and six layers of platelets through the thickness. Platelet thickness, t_p, was varied for some coupons. To control thickness of platelets, various numbers of AS4/PEKK plies (1–4) were assembled together to represent a single platelet. A platelet uniform overlap length through the thickness of the coupon was equal to the one-half of a platelet length, $L_{ov} = 0.5L_p$. The molding temperature/pressure conditions were as recommended by the manufacturer.

Effective (macroscopic) stress-strain curves for several tensile coupons are shown in Fig. 13. The experimental strength of the tensile coupons is shown in Fig. 14, where each point corresponds to a single coupon. In Fig. 14, platelet length-to-thickness aspect ratio was determined by dividing the nominal platelet length by the processed platelet thickness, which was obtained by dividing the measured average coupon thickness by the number of platelets in the coupon through thickness direction. The failure stress was calculated by dividing the load (N) at failure by the coupon cross-sectional area (specimen width multiplied by thickness). The strength enhancement with increased length-to-thickness ratio of a platelet can be seen in Fig. 14, where all the results (shown in solid black diamonds) were normalized with respect to the tensile strength of the AS4/PEKK UD CF tape. For large length-to-thickness platelet aspect ratio, the specimens failed by uniaxial tensile failure of the platelet, Fig. 15. For a smaller length-to-thickness platelet aspect ratio, the specimen tensile failure was caused by platelet delamination thereby leaving the platelets undamaged. Fig. 14 also reports the data points (open circles) for the tensile bars made of T800S/3900-2B carbon/epoxy staggered platelets, obtained from Taketa et al. [56] and the behavioral trends matches quite well with the data from the present work.

5. Conclusions

The stress-strain response of a meso-structure consisting of staggered and aligned platelets, parallel to each other and the loading axis, was studied. A three-dimensional, periodic RVE-based model was developed for the analysis of meso-structure deformation and progressive damage. The analysis accounted for the explicit interaction between the platelets with varying overlap geometries by modeling both platelets and platelet-platelet interfaces. Meso-structure geometries were identified that isolated platelet fracture and platelet-to-platelet delamination although both mechanisms were allowed to occur simultaneously. A continuum damage mechanics model was successfully utilized for modeling the initiation and evolution of damage in the meso-structure. Delamination of the interface was captured by employing a cohesive zone model.

The critical length-to-thickness ratio of the platelet is shown to be a manifestation of efficient platelet-to-platelet load transfer. The maximum strength of a given meso-structure is achieved at the critical length-to-thickness ratio, which produces platelet rupture as the primary failure mechanism, thereby extracting the greatest contribution from the platelet to meso-structure strength. Additional increase of platelet length-to-thickness ratio beyond the critical value is not accompanied by further increase in meso-structure strength. Below the critical length-to-thickness ratio, interfacial damage and platelet delamination limit the meso-structure strength.

The critical length-to-thickness ratio of a platelet was shown to be determined by the morphology of the meso-structure (i.e. the arrangement of overlap lengths). This revealed that the scatter of tensile strength of a platelet-arrayed meso-structure is related to its morphology variability and this variability can be mitigated by increasing the apparent length-to-thickness ratio of the platelet.

Acknowledgement

This work was supported by the Boeing Company. The authors are thankful to Dr. William B. Avery for the discussions and constructive criticism.

Appendix A

Fig. A1 and Table A1 summarize the geometrical parameters of considered meso-structure samples (RVEs).

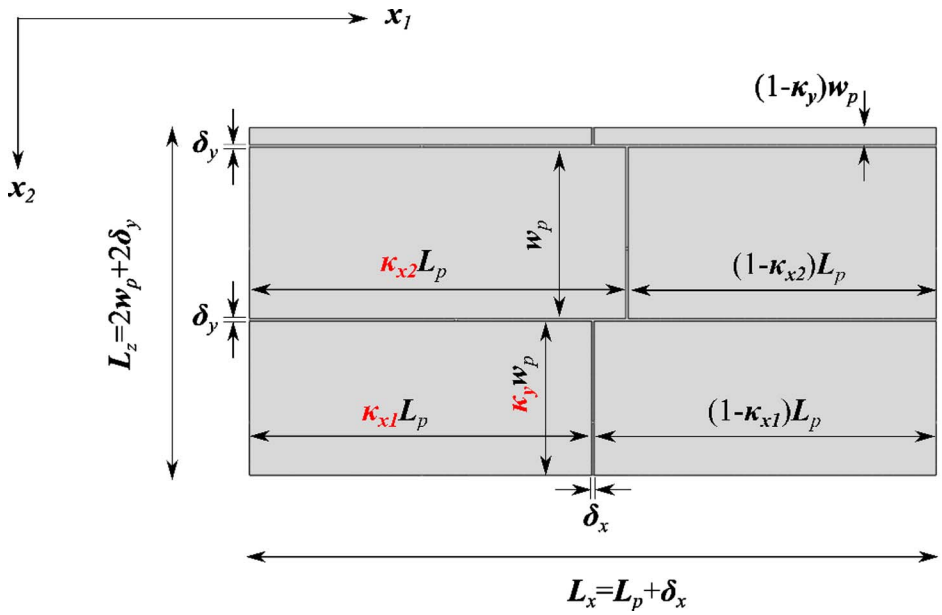

Fig. A1. Parametrized geometry of an RVE layer. (For interpretation of the references to colour in this figure legend, the reader is referred to the web version of this article.)

Table A1
Geometrical parameters of meso-structure samples (RVEs).

Meso-structure ID	Top/bottom layers			Middle layer		
	$\kappa_{x1}^{(t/b)}$	$\kappa_{x2}^{(t/b)}$	$\kappa_{y}^{(t/b)}$	$\kappa_{x1}^{(m)}$	$\kappa_{x2}^{(m)}$	$\kappa_{y}^{(m)}$
#1	0.75	0.2	0.4	0.4	0.6	0.1
#2	0.25	0.3	0.3	0.4	0.55	0.9
#3	0.2	0.1	0.85	0.75	0.35	0.45
#4	0.75	0.2	0.4	0.4	0.6	0.1
#5	0.2	0.55	0.25	0.75	0.35	0.45
#6	0.25	0.3	0.3	0.5	0.55	0.9

References

[1] Courtney T. Fundamental structure-property relationships in engineering materials. In: ASM handbook: materials selection and design, vol. 20; 1997. p. 336–56.
[2] Pech-Canul MI, Kongoli F. The modified central paradigm of materials science and engineering in the extraction and development of new and recycled materials. Miner Process Extract Metall 2016;125(4):238–41.
[3] Lakes R. Materials with structural hierarchy. Nature 1993;361:511–5.
[4] Selezneva M. Experimental and theoretical investigations of mechanical properties of randomly-oriented strand (ROS) composites PhD thesis McGill University; 2015
[5] Feraboli P, Peitso E, Deleo F, Cleveland T. Characterization of prepreg-based discontinuous carbon fiber/epoxy systems. J Reinf Plast Comp 2009;28(10):1191–214.
[6] van Wijngaarden M, Jongbloed A, de Vries J. Thermoplastic compound compression molding. In: SAMPE, Seattle, WA, USA; 2010.
[7] Eguemann N, Giger L, Roux M, Dransfeld C, Thiebaud F. Compression moulding of complex parts for the aerospace with discontinuous novel and recycled thermoplastic composite materials. In: 19th International conference on composite materials; 2013.
[8] Han JH, Alexander WTF, Greene T. Effect of fabric reinforcement on failure response of discontinuous long fiber composite bolted joints. In: SAMPE, Long Beach, CA, USA; 2011.
[9] Wan Y, Takahashi J. Tensile and compressive properties of chopped carbon fiber tapes reinforced with different fiber lengths and molding pressures. Composites A 2016;87:271–81.
[10] Wan Y, Takahashi J. Tensile properties and aspect ratio simulation of transversely isotropic discontinuous carbon fiber reinforced thermoplastics. Compos Sci Technol 2016;137:167–76.
[11] Yamashita S, Hashimoto K, Suganuma H, Takahashi J. Experimental characterization of the tensile failure mode of ultra-thin chopped carbon fiber tape-reinforced thermoplastics. J Reinf Plast Compos 2016;35(18):1342–52.
[12] Yamashita S, Sonehara T, Takahashi J, Kawabe K, Murakami T. Effect of thin-ply on damage behaviour of continuous and discontinuous carbon fibre reinforced thermoplastics subjected to simulated lightning strike. Compos A Appl Sci Manuf 2017;95:132–40.
[13] Nicoletto G, Riva E, Stocchi A. Mechanical characterization of advanced random discontinuous carbon/epoxy composites. Mater Today: Proc 2016;3(4):1079–84.
[14] Abdul Rasheed M, Hattum FV, Rietman B, Visser H, Akkerman R. Effect of overlap length on the mechanical properties of flake reinforced thermoplastic composites. In: CAMAX conference proceedings, October 26-29, Dallas, TX; 2015.
[15] Bonderer JJ, Studart A, Gauckler LJ. Bioinspired design and assembly of platelet reinforced polymer films. Science 2008;319:1069–73.
[16] Hsueh C-H. A two-dimensional stress transfer model for platelet-reinforcement. Compos Eng 1994;4(10):1033–43.
[17] Mendels A-A, Leterrier Y, Manson J-AE. Stress transfer model for single fibre and platelet composites. J Comp Mater 1999;33:1525–43.
[18] Kotha S, Kotha S, Guzelsu N. A shear-lag model to account for interaction effects between inclusions in composites reinforced with rectangular platelets. Compos Sci Technol 2000;60:2147–58.
[19] Fattahi A, Mondali M. Theoretical study of stress transfer in platelet reinforced composites. J Theor Appl Mech 2014;52:3–14.
[20] Bar-On B, Wagner HD. Effective moduli of multi-scale composites. Comp Sci Tech 2012;72:566–73.
[21] Padawer G, Beecher N. On the strength and stiffness of planar reinforced plastic resins. Polym Eng Sci 1970;10(3):185–92.
[22] Glavinchevski B, Piggott M. Steel disc reinforced polycarbonate. J Mater Sci 1973;8:1373–82.
[23] Jackson A, Vincent J, Turner R. The mechanical design of nacre. Proc R Soc Lond 1988;B 234:415–40.
[24] Wyser Y, Leterrier Y, Manson J-AE. Analysis of failure mechanisms in platelet-reinforced composites. J Mater Sci 2001;36:1641–51.
[25] Barthelat F, Tang H, Zavattieri P, Li C-M, Espinosa H. On the mechanics of mother-of-pearl: a key feature in the material hierarchical structure. J Mech Phys Solids 2007;55:306–37.
[26] Begley M, Philips BNR, Compton D, Wilbrink R, Ritchie, Ultz M. Micromechanical models to guide the development of synthetic 'brick and mortar' composites. J Mech Phys Sol 2012;60:1545–60.
[27] Pimenta S, Robinson P. An analytical shear-lag model for composites with 'brick-and-mortar' architecture considering non-linear matrix response and failure. Comp Sci Tech 2014;104:111–24.
[28] Taketa I, Okabe T, Kitano A. A new compression-molding approach using unidirectionally arrayed chopped strands. Composites A 2008;39:1884–90.
[29] Xue J, Wang W-X, Zhang J-Z, Wu S-J. Progressive failure analysis of the fiber metal laminates based on chopped carbon fiber strands. J Reinf Plast Comp 2015;34(5):364–76.
[30] Xue J, Wang W-X, Hu J-F, Zhang J-Z, Wu S-J. Influence of fiber length of the tensile behavior of fiber metal laminates with discontinuous reinforcement. J Reinf Plast Comp 2015.
[31] Böhm HJ. A short introduction to basic aspects of continuum micromechanics. ILSB reports/ILSB-Arbeitsbericht 206, Vienna; 2012.
[32] Suquet P. Elements of homogenization theory for inelastic solid mechanics. In: Homogenization techniques for composite media. Berlin: Springer-Verlag; 1987. p. 194–275.
[33] Ostoja-Starzewski M. The use, misuse, and abuse of stochastic random media. In: Proceedings of European conference on computational mechanics; 2001.
[34] Cox H. The elasticity and strength of paper and other fibrous materials. Brit J Appl Phys 1952;3:72–9.
[35] Davila CG, Leone FA. Analysis methods for progressive damage of composite structures. Technical report NASA/TM-2013-218024; 2013.
[36] Lapczyk I, Hurtado J. Progressive damage modeling in fiber-reinforced materials. Composites A 2007;38:2333–41.
[37] Camanho P, Davila C. Mixed-mode decohesion elements for the simulation of delamination in composite materials. NASA/TM-2002-211737; 2002.
[38] Song K, Li Y, Rose C. Continuum damage mechanics models for the analysis of progressive failure in open-hole tension laminates. In: AIAA; 2011.
[39] Hallett S, Green B, Jiang W, Wisnom M. An experimental and numerical investigation into the damage mechanisms in notched composites. Composites A 2009;40:613–24.
[40] Talreja A. A continuum mechanics characterization of damage in composite materials. Proc R Soc Lond A 1985;399:195–216.
[41] Chaboche J. Continuous damage mechanics –a tool to describe phenomena before crack initiation. Nucl Eng Des 1981;64:233–47.
[42] Krajcinovic D. Damage mechanics. Mech Mater 1989;8:117–97.
[43] Naderi M, Khonsari M. Stochastic analysis of inter-and intra-laminar damage in notched PEEK laminates. Exp Polym Lett 2013;7:383–95.
[44] Reeder J, Crews J. Mixed-mode bending method for delamination testing. AiAA J 1990;28(7):1270–6.
[45] Jain J, Ghosh S. Homogenization based 3D continuum damage mechanics model for composites undergoing microstructural debonding; 2008.
[46] Forghani A, Shahbazi M, Zobeiry N, Poursartip A, Vaziri R. An overview of continuum damage models used to simulate intralaminar failure mechanisms in advanced composite materials. In: Numerical modeling of failure in advanced composite materials, Elsevier; 2015.
[47] Dassault Systèmes. ABAQUS (2016) ABAQUS Documentation, Providence, RI.
[48] Matzenmiller A, Lubliner J, Taylor R. A constitutive model for anisotropic damage in fiber-composites. Mech Mater 1995;20:125–52.
[49] Hashin Z. Failure criteria for unidirectional fiber composites. J Appl Mech 1980;47:329–34.
[50] Bazant Z, Oh B. Crack band theory for fracture of concrete. Mater Struct 1983;16:155–77.
[51] Czabaj M, Ratcliffe J. Comparison of intralaminar and interlaminar mode-I fracture toughness of unidirectional IM7/8552 graphite/epoxy composite. In: American society for composites 27th technical conference, Arlington, TX; 2012.
[52] Pinho ST, Robinson P, Iannucci L. Fracture toughness of the tensile and compressive fibre failure modes in laminated composites. Compos Sci Technol 2006;66(13):2069–79.
[53] Davilla CG, Camanho P, Turon A. Effective simulation of delamination in aeronautical structures using shells and cohesive elements. J Aircrafts 2008;45(2).
[54] Brewer J, Lagace P. Quadratic stress criterion for initiation of delamination. J Comp Mater 1988;22(12):1141–55.
[55] Whitcomb J. Analysis of Instability-related growth of through-thickness delamination. NASA TM-86301.
[56] Taketa I, Koyanagi A, Matsutani H. Effect of fiber length on the tensile strength of unidirectionally arrayed chopped strands. In: 20th International conference on composite materials, Copenhagen; 2015.